PHOTONICS Research

Generation and modulation of non-classical light in a strongly coupled photon–emitter system

Lingxiao Shan,[1] Juanjuan Ren,[1] Qi Zhang,[1] Qi Liu,[1,2] Yun Ma,[1] Qihuang Gong,[1,2,3,4] and Ying Gu[1,2,3,4,*]

[1]State Key Laboratory for Mesoscopic Physics, Department of Physics, Peking University, Beijing 100871, China
[2]Frontiers Science Center for Nano-optoelectronics & Collaborative Innovation Center of Quantum Matter & Beijing Academy of Quantum Information Sciences, Peking University, Beijing 100871, China
[3]Collaborative Innovation Center of Extreme Optics, Shanxi University, Taiyuan 030006, China
[4]Peking University Yangtze Delta Institute of Optoelectronics, Nantong 226010, China
*Corresponding author: ygu@pku.edu.cn

Received 19 November 2021; revised 19 January 2022; accepted 22 February 2022; posted 22 February 2022 (Doc. ID 449106); published 25 March 2022

Non-classical light, especially its single photon and squeezing properties, plays a fundamental role in on-chip quantum networks. The single photon property has been widely studied in photonic cavities including photonic crystals (PhCs), micropillar cavities, nanowires, and plasmonic cavities. However, the generation and modulation of squeezing light in nanophotonic cavities remain to be explored. Here, we theoretically demonstrate a strongly coupled PhC–plasmonic-emitter system enabling non-classical light generation and modulation. The hybridization of a PhC waveguide and an Ag nanoparticle forms a band-edge mode with a narrow linewidth and a strong confined field, which enables strong light–emitter interaction, further resulting in simultaneous generation of squeezing and single photon properties for on-chip applications. Non-classical light emission can be modulated with the detuning between the band-edge mode and the emitter. The emission is efficiently channeled by the PhC waveguide with a high coupling efficiency, accompanying unidirectional transmission under excitation by a circularly polarized emitter. The system provides a candidate for tunable and bifunctional on-chip non-classical light sources at the nanoscale and may offer more possibilities to build versatile quantum networks.

https://doi.org/10.1364/PRJ.449106

1. INTRODUCTION

Non-classical light is widely studied for on-chip light sources in quantum applications such as quantum computing, quantum metrology, and quantum sensing [1,2]. Non-classical light with a single photon property [3], photon entanglement [4], or squeezing property [5–8] can be generated in cavity quantum electrodynamic systems with an emitter and a microcavity. When the interaction between the emitter and the cavity mode is stronger than the cavity loss and emitter decay, the light–matter interaction reaches the strong coupling regime [9], which can be utilized to produce non-classical light with single photon and squeezing properties. The mechanism of single photon generation is a "photon blockade," that is, the excitation of the first photon will decrease the possibility of exciting the second photon [10,11]. Additionally, the squeezing property, denoting quantum light with reduced quantum noise, can also be achieved in the strong coupling regime [12].

To date, photonic cavities have achieved ultrahigh quality factors [11,13–17] or ultrasmall mode volumes [18–20]; thus the strong coupling regime can be reached [21,22] in various structures including photonic crystals (PhCs) [14,23–25], micropillar cavities [26–28], whisper-gallery-mode microresonators [29–31], and plasmonic cavities [18,19,32–34]. In the past decade, photonic cavities equipped with quantum dots have attracted much attention in on-chip applications. Particularly, single photon sources are widely studied in on-chip devices with high-quality-factor microcavities, where strong coupling induces the photon blockade, and the detuning between atom and field can modulate the single photon property [35–40]. However, the generation of squeezing light by strong coupling in photonic cavities has not been fully explored and needs further progress, especially in on-chip devices. It would benefit precise measurement for quantum metrology [1] and light sources for quantum computing [2]. People have used plasmonic cavities [41] and micropillar cavities [28] to improve squeezing properties [42] by suppressing shot noise. But in the above studies, non-classical light emission couples only to free space. Aiming for a more compact and versatile quantum network, more advances are still needed for the on-chip generation and modulation of squeezing light.

In the present work, we propose a hybrid PhC–plasmonic system for on-chip generation and modulation of non-classical light. Hybridization between the band edge of a PhC waveguide and surface plasmons produces a band-edge mode with strong light confinement and a narrow linewidth with 3 meV, which ensures strong coupling. Thus, squeezing light and single photon emission can be simultaneously produced in the hybrid system. Especially, the squeezing light property is sensitive to loss, so the suppressed decay in strong coupling is beneficial to the generation of squeezing light. The strongly confined field provided by the AgNP also contributes to enhancement of the brightness of non-classical light output. Modulation of non-classical light is conducted by tuning the resonance of the band-edge mode, which can be realized by such methods as temperature tuning and current tuning [43]. The second-order correlation function $g^{(2)}(0)$ falls to a level lower than 10^{-1} due to the photon blockade effect, and the degree of squeezing reaches 0.29 dB. Photon out-coupling is also convenient in that 70% of total emission can be channeled through the PhC waveguide, and furthermore, unidirectional transmission can be achieved under excitation of a circularly polarized emitter. The hybrid system provides a method to improve on-chip generation and modulation of non-classical light especially with a squeezing property. It offers possibilities to build multifunctional non-classical light sources for on-chip quantum sensing and metrology and would benefit scalable quantum networks.

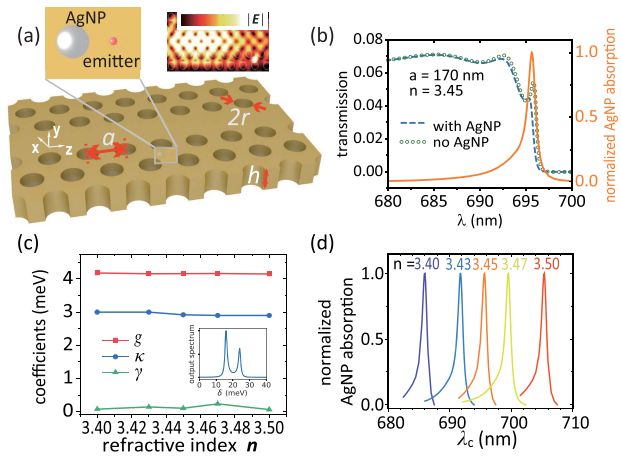

Fig. 1. (a) Schematic diagram of the strongly coupled photonic-crystal–plasmonic-emitter system. The inset depicts the electric field profile of the band-edge mode. (b) Calculated absorption spectrum of AgNP (orange solid curve), and transmission spectra of the system with AgNP (blue dashed curve) and without AgNP (green dotted curve). (c) Coupling strength g, cavity decay rate κ, and emitter decay rate γ as functions of the refractive index n. The inset depicts the output spectrum from transmitted photon $S(\delta) \propto \frac{1}{\pi}\mathrm{Re}\int\langle a^{\dagger}(\tau)a(0)\rangle e^{i\delta\tau}\mathrm{d}\tau$ showing Rabi splitting. δ is the detuning between the transmitted photon and the pump field. (d) Normalized AgNP absorption spectra under varied refractive indices ($n = 3.40$–3.50) of PhC materials, which describes the shift of the band-edge mode.

2. MODEL SETUP OF THE STRONGLY COUPLED PHOTONIC-CRYSTAL–PLASMONIC-EMITTER SYSTEM

Our proposed system contains a PhC waveguide, a silver nanoparticle (AgNP), and a two-level emitter [Fig. 1(a)]. In the PhC structure, a line defect is introduced by removing an entire row of air holes in a hexagonal lattice, which supports guided modes. The AgNP is buried in the PhC lattice region. The field coupling between the PhC and AgNP produces a band-edge mode, which can be clearly seen in the absorption spectrum of the AgNP [44] [Fig. 1(b)]. For the band-edge mode, the PhC waveguide intensely couples with the AgNP, possessing a very high local density of states at its band edge. Note that it is not necessary to set the AgNP in resonance to produce the band-edge mode. Actually, the resonances of a single AgNP without a PhC waveguide lie far away from the band edge (~695 nm). The band-edge mode demonstrates a remarkable suppression of the linewidth and possesses a strongly confined field around the nanoparticle and in the waveguide, which can be regarded as a single high-quality microcavity hybridized by the PhC waveguide and the AgNP. We consider only the system close to the resonance of the band-edge mode, so other coupling terms between the AgNP and PhC waveguide can be neglected. It is worth mentioning that our system treats mode hybridization differently from other hybrid systems [45–47]. In their systems, mode hybridizations occur between a narrow-linewidth cavity mode and a plasmonic mode (or two narrow-linewidth cavity modes), and they treat the hybridization with two coupled modes. The situation is different in our system where hybridization happens at the band edge of the PhC. Therefore, the two-level emitter placed near the AgNP can strongly interact with the band-edge mode, enabling the system to reach the strong coupling regime. In such a condition, the system can produce non-classical light with single photon and squeezing properties. The suppressed decays κ and γ benefit the squeezing property sensitive to noises, and the strong field confinement around AgNP enhances the brightness of non-classical light output. The detuning between the band-edge mode and the emitter can be exploited to modulate non-classical light properties. As shown in the inset of Fig. 1(b), the field profile of the band-edge mode mainly stays in the line defect region, so it is a convenient channel for photon out-coupling in non-classical light sources.

The photon–emitter interaction system is generally described by the Jaynes–Cummings model under dipole and rotating wave approximations [5]. The system Hamiltonian is expressed as $\mathcal{H} = \Delta_c a^{\dagger}a + \Delta_a\sigma_+\sigma_- + g(a\sigma_+ + a^{\dagger}\sigma_-) + \mathcal{E}(\sigma_+ + \sigma_-)$ ($\hbar = 1$) under the interaction picture. Here, $g = \vec{\mu}\cdot\vec{E}_{\mathrm{mode}}$ denotes the coupling strength between the emitter dipole $\vec{\mu}$ and the band-edge mode $\vec{E}_{\mathrm{mode}}$. $\Delta_a = \omega_a - \omega$ and $\Delta_c = \omega_c - \omega$ denote emitter–pump and cavity–pump detuning, respectively, where ω_a, ω_c, and ω are the frequency of the emitter, the cavity mode, and the pump field [Fig. 2(a)], respectively. $\sigma_{\pm}$ denote the raising and lowering operators of the two-level emitter, and a and $a^{\dagger}$ represent the annihilation and creation operators of the cavity mode, respectively. A pump field is introduced to excite the atom with $\mathcal{E} = \vec{\mu}\cdot\vec{E}_{\mathrm{pump}}$ denoting the coupling strength between the pump field $\vec{E}_{\mathrm{pump}}$ and the dipole of the emitter $\vec{\mu}$. When decays to the outer environment are considered, the dynamics of the system is governed by the master equation [5]

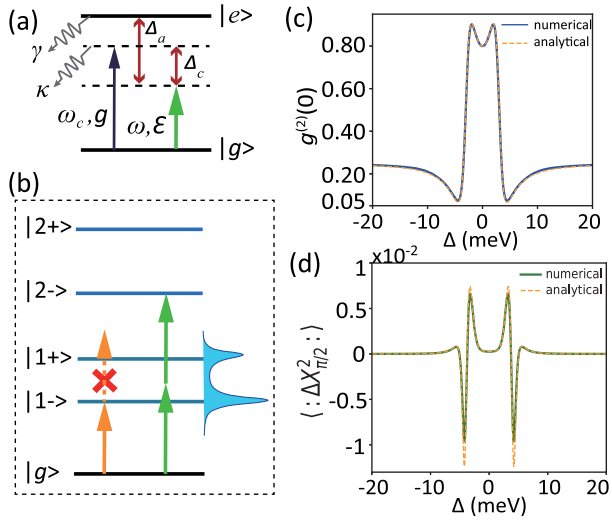

Fig. 2. Generation of non-classical light with single photon and squeezing properties. (a) Energy-level diagram of the system. Δ_a (Δ_c) is the detuning between the emitter ω_a (band-edge mode ω_c) and pump light ω. $g, \mathcal{E}$ represent mode–emitter and pump–emitter couplings. κ, γ denote decays from the mode and emitter. (b) Dressed states of the effective Hamiltonian. Orange (green) arrow denotes that the first photon is resonant (off resonance) with the cavity–emitter system, and the subsequent photon is prohibited (permitted) because it is off (in) resonance with higher dressed states. (c) Calculated second-order correlation function $g^{(2)}(0)$ and (d) normal-ordered quadrature fluctuation $\langle :\Delta X^2_{\pi/2}: \rangle$ from master equation with Quantum Toolbox in Python (solid curve) and from analytical solution [Eqs. (4) and (5)] of effective Hamiltonian (dashed curve).

$$\dot{\rho} = i[\rho, \mathcal{H}] + \frac{\gamma}{2}(2\sigma_-\rho\sigma_+ - \sigma_+\sigma_-\rho - \rho\sigma_+\sigma_-) + \frac{\kappa}{2}(2a\rho a^\dagger - a^\dagger a\rho - \rho a^\dagger a), \quad (1)$$

where κ, γ are decay rates from the cavity mode and the emitter, respectively. The mode–emitter coupling strength g reaches a high level under a strongly confined field around the AgNP. κ is extracted from the narrow linewidth of the absorption spectrum of the band-edge mode, where the absorption is the dominant factor of κ, surpassing the small scattering part from the PhC waveguide [44]. Additionally, γ is suppressed because the photonic bandgap of the PhC waveguide inhibits many radiation modes. Therefore, the interaction between the emitter and the band-edge mode can reach the strong coupling regime ($g > \kappa, \gamma$). In this system, the single photon can be generated because of the photon blockade effect; simultaneously, the squeezing properties occur under appropriate emitter–cavity detunings.

To guarantee strong coupling between the emitter and the band-edge mode, we set up our system with the following parameters. The lattice period of the PhC waveguide a is 170 nm, the diameter of air holes is $2r = 98.6$ nm, and the width of the PhC layer is $h = 142.8$ nm. The refractive index of the PhC is $n = 3.45$. Here, r is chosen as $r/a = 0.29$ to match the emitter wavelength (695 nm) and the band edge of PhC. The width h is set at $h/a = 0.84$ in the range where only one transverse mode along y axis exists. The fabrication error can be tolerated when the variation of the photonic band diagram is not comparable with the emitter wavelength variation. An AgNP buried in the PhC lies a row below the line defect, between two air holes in the lattice region [Fig. 1(a)]. This position can achieve the strongest photon–emitter coupling strength g. The precise position of the AgNP has an influence on the decay of the cavity mode κ. From Ref. [44], the deviation within 50 nm can be tolerated with only 0.8 meV variation of κ. The radius of the AgNP is 7 nm, and the silver permittivity in the visible region adopts the data from Johnson and Christy [48] in 1972. A two-level emitter is placed near the AgNP with a spacing $d = 2$ nm, and its dipole moment is set as $\mu = 1e$ nm. The relative position between the AgNP and the emitter should be close enough for very strong field enhancement. The azimuthal position of the emitter also has a slight modulation of γ [44]. Such nanometer accuracy of assembling and positioning is possible with scanning tunneling microscopy or DNA origami technology [9,49].

With the above parameters, we use commercial COMSOL software to simulate coefficients g, κ, γ in the photon–emitter interaction (details in Appendix A). The coupling strength g between the emitter and the band-edge mode reaches 4.2 meV near the AgNP. The mode displays a strongly suppressed linewidth ($\kappa = 2.9$ meV) compared to the dipole mode of a single AgNP (~20 meV) [44], and the decay from the emitter γ is lower than 1 meV. Therefore, the condition for strong coupling $g > \kappa, \gamma$ is satisfied [Fig. 1(c)]. Rabi splitting from strong mode–emitter coupling can be seen in the output spectrum from the transmitted photon $S(\delta) \propto \frac{1}{\pi}\mathrm{Re}\int \langle a^\dagger(\tau)a(0)\rangle e^{i\delta\tau}\mathrm{d}\tau$ as shown in the inset of Fig. 1(c). The band-edge mode is located at 695 nm when the refractive index n is 3.45. When the refractive index ranges from 3.40 to 3.50, the resonance moves from 685 nm to 705 nm (in a 50 meV range) [Fig. 1(d)]. Under such varied wavelengths of the band-edge mode, the single photon and squeezing properties can be modulated. In our system, modulation of a non-classical system requires the mode shift of ~0.7 nm (1 meV), which can be obtained with temperature tuning [50] in III–V semiconductors such as AlGaAs [51] under 30 K. When the wavelength of the band-edge mode varies, g, κ, γ remain stable in modulation range without influence by changing the refractive index [Fig. 1(c)]. Therefore, we adapt the average when the band-edge mode shifts with $g = 4.2$ meV, $\kappa = 2.9$ meV, and $\gamma = 0.2$ meV.

3. GENERATION AND MODULATION OF NON-CLASSICAL LIGHT

With the strongly coupled photon–emitter system above, we obtain non-classical light with single photon and squeezing properties. As shown in Figs. 2(c) and 2(d), the second-order correlation function $g^{(2)}(0)$ can be lower than 0.1, and the degree of squeezing reaches 0.18 dB. To discuss the underlying mechanism, we study the steady-state properties of our system. An effective Hamiltonian is employed to describe the evolution of the system under dissipations:

$$\mathcal{H}_{\mathrm{eff}} = (\Delta_c - i\kappa/2)a^\dagger a + (\Delta_a - i\gamma/2)\sigma_+\sigma_- + g(a\sigma_+ + a^\dagger\sigma_-) + \mathcal{E}(\sigma_+ + \sigma_-). \quad (2)$$

It is non-Hermitian because of added imaginary dissipation terms in the frequency of the emitter and the band-edge mode. The atom–photon states are denoted as $|s,m\rangle$. $s \in \{e,g\}$ denotes excited or ground level of the emitter, and m denotes photon number of the band-edge mode.

The energy of dressed states $|m\pm\rangle$ of the effective Hamiltonian is ($m \geqslant 1$) (details in Appendix C)

$$\tilde{\Delta}_{m\pm} = (m-1)\tilde{\Delta}_c + \frac{\tilde{\Delta}_c + \tilde{\Delta}_a}{2} \pm \frac{1}{2}\sqrt{(\tilde{\Delta}_c - \tilde{\Delta}_a)^2 + 4mg^2}, \tag{3}$$

where $\tilde{\Delta}_a = \Delta_a - i\gamma/2$ and $\tilde{\Delta}_c = \Delta_c - i\kappa/2$. Equation (3) is applicable for all quantum excitations [52]. Here, the anharmonic spacings between energy levels result in the photon blockade and bunching effect [10,11]. As shown in Fig. 2(b), when the first photon is resonant with the first rung of eigenenergies $|1+\rangle$ or $|1-\rangle$, the second photon will be detuned from the second rung $|2+\rangle$ or $|2-\rangle$. Thus the first photon "blocks" the entry of the second photon. If two-photon excitation is resonant with the second rung, the system tends to absorb two photons together. This situation corresponds to photon bunching, shown as a peak in $g^{(2)}(0)$.

Figure 2(c) demonstrates the single photon with varying wavelengths of pump light. Here, we set the band-edge mode and the emitter in resonance ($\Delta_a = \Delta_c = \Delta$), so the pump light with a detuning Δ can modulate non-classical light properties. The solid curves are obtained from numerical calculation of master equation [Eq. (1)] under the Quantum Toolbox in Python [53,54]. Figure 2(c) shows that $g^{(2)}(0) < 0.1$ can be obtained under appropriate detunings Δ. Such a property can be used as high-quality single photon emission [55]. The minima of $g^{(2)}(0)$ are achieved when the pump is resonant ($\Delta \simeq \pm g$) with the first rungs of dressed states $\tilde{\Delta}_{1-}, \tilde{\Delta}_{1+}$, which demonstrates the photon blockade effect [11]. Moreover, the minimum does not equal zero because a small fraction of two-photon excitation is permitted by cavity and emitter decays (details in Appendix D). $g^{(2)}(0)$ gets peak values when $2\Delta \simeq \pm\sqrt{2}g$. In this situation, the pump is resonant with the second rungs of dressed states in that the system has a higher probability of capturing two photons simultaneously [11] as shown with green arrows in Fig. 2(b).

The squeezing property is depicted in Fig. 2(d) with normal-ordered quadrature fluctuation $\langle{:}\Delta X_\theta^2{:}\rangle = -\langle{:}(\Delta a^\dagger e^{-i\theta} - \Delta a e^{i\theta})^2{:}\rangle/4$, where $\Delta a\,(\Delta a^\dagger)$ represents the fluctuation operator of the mode field $a - \langle a\rangle\,(a^\dagger - \langle a^\dagger\rangle)$. $\langle{:}\Delta X_\theta^2{:}\rangle < 0$ indicates that photon squeezing exists. θ is a tunable phase of a local oscillator, and we choose $\theta = \pi/2$ to obtain the maximum degree of squeezing. When $\Delta = \pm g = \pm 4.2$ meV, the degree of squeezing $10\log_{10}(\langle\Delta X_{\pi/2}^2\rangle/\langle\Delta X^2\rangle_{\text{vacuum}}) = 0.18$ dB for quadrature operators, and the single photon property is best with $g^{(2)}(0) = 0.081$. Here, the squeezing property is generated along with single photon properties in appropriate detunings, which makes an on-chip single photon and squeezing light source possible.

The results above can also be achieved in analytical solutions in low-excitation subspaces with no more than two quanta. It is reasonable when the pump is very weak compared to the decay of the band-edge mode (here, $\mathcal{E}/\kappa = 0.1$). As shown in Figs. 2(c) and 2(d), the analytical results are in accordance with numerical solutions. The energy eigenstates of the subspace are denoted as $|s,m\rangle$. $s \in \{e,g\}$ denotes excited or ground level of the emitter, and $m \in \{0,1,2\}$ denotes the photon number of the band-edge mode. A state in the subspace reads $|\psi\rangle = c_{g0}|g0\rangle + c_{g1}|g1\rangle + c_{e0}|e0\rangle + c_{g2}|g2\rangle + c_{e1}|e1\rangle$ with probability amplitudes $c_{s,m}$. The non-classical light properties can be obtained as

$$g^{(2)}(0) = \frac{\langle a^{\dagger 2}a^2\rangle}{\langle a^\dagger a\rangle^2} = \frac{2|c_{g2}|^2}{|c_{g1}|^4} = \left|\frac{\tilde{\Delta}_{1-}\tilde{\Delta}_{1+}}{\tilde{\Delta}_{2-}\tilde{\Delta}_{2+}}\right|^2, \tag{4}$$

$$\begin{aligned}\langle{:}\Delta X_\theta^2{:}\rangle &= \frac{1}{2}\mathrm{Re}[e^{-2i\theta}\langle\Delta a^2\rangle] + \frac{1}{2}\langle\Delta a^\dagger \Delta a\rangle \\ &= \frac{1}{2}\mathcal{E}^2 g^2 \mathrm{Re}\left[e^{-2i\theta}\frac{\tilde{\Delta}_c^2}{\tilde{\Delta}_{2-}\tilde{\Delta}_{2+}\tilde{\Delta}_{1-}^2\tilde{\Delta}_{1+}^2}\right] \\ &\quad + \mathcal{E}^4 g^2 \frac{g^2 + |\tilde{\Delta}_c|^2}{|\tilde{\Delta}_{1-}\tilde{\Delta}_{1+}|^4}.\end{aligned} \tag{5}$$

It can be seen that the expression of $\langle{:}\Delta X_\theta^2{:}\rangle$ has some higher-order terms of $\mathcal{E}$. They dominate in photon squeezing when a large fraction of population resides in $|g1\rangle$ and $|e0\rangle$, particularly under a photon blockade (details in Appendix C).

Next, we introduce the refractive index tuning to study further non-classical modulation in our system. Here, we change the refractive index of PhC materials near 3.45 so that the band-edge mode ω_c will shift with the photonic bandgap [Fig. 1(d)]. Figure 3 depicts modulation of the single photon and squeezing properties when Δ_a, Δ_c vary in a 20 meV range. From the effective Hamiltonian [Eq. (2)], the detunings $\Delta_a = \omega_a - \omega$ and $\Delta_c = \omega_c - \omega$ can be independently tuned. As shown in Fig. 3(a), the better single photon property appears when $\Delta_c \neq \Delta_a$, depicted by dark regions. It also originates from the photon blockade when the pump is in resonance with the

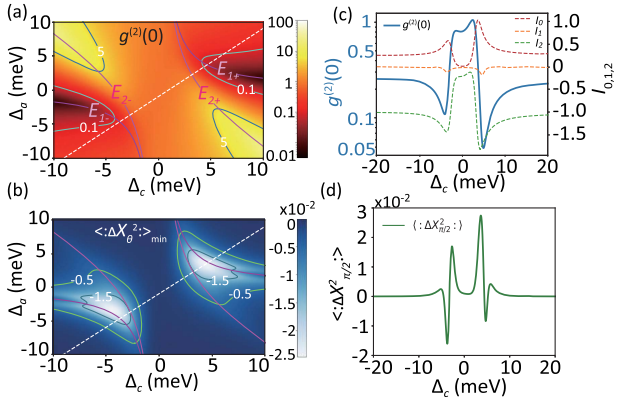

Fig. 3. (a) Calculated second-order correlation function $g^{(2)}(0)$ and (b) minima of normal-ordered quadrature fluctuation $\langle{:}\Delta X_\theta^2{:}\rangle_{\min}$ versus cavity–pump detuning Δ_c and emitter–pump detuning Δ_a. First and second rungs of dressed states $E_{1\pm}, E_{2\pm}$ are marked by purple curves. (c) Second-order correlation function $g^{(2)}(0)$ and fluctuation correlation functions I_0, I_1, I_2 with varied Δ_a when $\Delta_c - \Delta_a = 0.95$ meV. (d) Squeezing properties for $\Delta_c - \Delta_a = 0.95$ meV. The optimal single photon and squeezing properties appear at $\Delta_c = -3.40$ meV and $\Delta_a = -4.35$ meV, which correspond to white dashed lines in (a) and (b).

first rungs of dressed states at $\omega = (\omega_c + \omega_a)/2 \pm \mathrm{Re}\sqrt{(\tilde{\Delta}_c - \tilde{\Delta}_a)^2/4 + g^2}$ ($\mathrm{Re}[\tilde{\Delta}_{1\pm}] = 0$). It can be verified by the eigenenergies marked in Fig. 3(a). Bright regions illustrate photon bunching effect with $g^{(2)}(0) > 1$ corresponding to two-photon excitation. It can be confirmed with the curve $2\omega = 3\omega_c/2 + \omega_a/2 \pm \mathrm{Re}\sqrt{(\tilde{\Delta}_c - \tilde{\Delta}_a)^2/4 + 2g^2}$ ($\mathrm{Re}[\tilde{\Delta}_{2\pm}] = 0$) shown in Fig. 3(a). In Fig. 3(c), for the balance between single photon and squeezing properties, $\Delta_c = -3.40$ meV and $\Delta_a = -4.35$ meV are chosen, where $g^{(2)}(0)$ approaches a low value 0.098, which reaches a low level [39,56]. In real systems, such detunings ($\Delta_c - \Delta_a = 0.95$ meV) can be achieved with temperature tuning in III–V semiconductor materials such as AlGaAs [43,50,51]. Under a photon blockade [shown by $E_{1\pm}$ in Fig. 2(a)] with larger detunings $\Delta_c - \Delta_a$, the single photon property can be better with $g^{(2)}(0) \sim 10^{-2}$. Moreover, the single photon and squeezing light output can be further optimized with a more confined field such as bow-tie resonators and gap plasmon structures [18,57], where the cavity decay κ can be further improved.

In Fig. 3(b), the squeezing property is measured by the minimum of normal-ordered quadrature fluctuation $\langle{:}\Delta X_\theta^2{:}\rangle_{\min} = -|\langle \Delta a^2 \rangle|/2 + \langle \Delta a^\dagger \Delta a \rangle/2$ when θ varies. When Δ_a is fixed at -4.35 meV, Fig. 3(d) displays the squeezing property as a function of Δ_c, where $\langle{:}\Delta X_\theta^2{:}\rangle_{\min}$ falls to -0.016 ($\mathcal{E}/\kappa = 0.2$, degree of squeezing 0.29 dB) at $\Delta_c = -3.40$ meV. Note that strong photon squeezing mainly appears near the photon blockade with $\mathrm{Re}[\tilde{\Delta}_{1\pm}] = 0$. Actually, photon squeezing is directly related to the single photon property in our system. The second-order correlation function can be expanded to some fluctuation correlation functions with orders of expectations $\alpha\,(\alpha^*) = \langle a \rangle\,(\langle a^\dagger \rangle)$ of field operators as $g^{(2)}(0) = 1 + I_0 + I_1 + I_2$ [7,8], where

$$
\begin{aligned}
I_0 &= \langle \Delta a^{\dagger 2} \Delta a^2 \rangle / \langle a^\dagger a \rangle^2, \\
I_1 &= 4\,\mathrm{Re}[\langle a^\dagger \rangle \langle \Delta a^\dagger \Delta a^2 \rangle] / \langle a^\dagger a \rangle^2, \\
I_2 &= \frac{2|\alpha|^2 \langle \Delta a^\dagger \Delta a \rangle + \alpha^{*2} \langle \Delta a^2 \rangle + \alpha^2 \langle \Delta a^{\dagger 2} \rangle}{\langle a^\dagger a \rangle^2} \\
&= |\alpha|^2 \frac{\langle {:}(\Delta a^\dagger e^{-i\theta} + \Delta a e^{i\theta})^2{:} \rangle}{\langle a^\dagger a \rangle^2} = 4|\alpha|^2 \frac{\langle {:}\Delta X_\theta^2{:} \rangle}{\langle a^\dagger a \rangle^2}.
\end{aligned} \tag{6}
$$

I_0 represents the normally ordered variance of fluctuation intensity, I_1 represents the normally ordered correlation between fluctuation amplitude and intensity, and I_2 is the normally ordered variance of the field quadrature operator. Here, I_2 corresponds to photon squeezing [7]. We demonstrate the second-order correlation function with fluctuation correlation functions in Fig. 3(c) when $\Delta_c - \Delta_a = 0.95$ meV, which comes from data on the white dashed line in Figs. 3(a) and 3(b). It can be seen how fluctuation correlations contribute to $g^{(2)}(0)$. I_1 is nearly zero over all regions except near the photon blockade. The two valleys of $g^{(2)}(0)$ under the photon blockade are mainly attributed to negative I_2. That means the single photon property stems from photon squeezing in our system, which is also applicable in similar cavity–emitter systems [7]. Thus, both single photon and squeezing light output can be achieved under a photon blockade. Moreover, compared to solid-state systems without photonic structures [42], strong coupling from the band-edge mode could further enhance photon squeezing. Additionally, at photon bunching, the absolute values of I_0, I_1, I_2 decrease; thus $g^{(2)}(0)$ is close to one, and the squeezing property fades (details in Appendix D).

Additionally, qubit–qubit entanglement can be achieved in our system. When a metallic nanoparticle acts as a mediation of the coupling between two emitters, the strong localized field around the nanoparticle can enhance the qubit–qubit entanglement in hybrid plasmonic–waveguide systems [58,59]. This situation may also be achieved when two emitters are located beside AgNP in our system under the more confined field.

4. TRANSMISSION OF NON-CLASSICAL LIGHT

The line defect enables fine guiding of transmitted light in our system, which provides a convenient channel for output of non-classical light. The fine transmission property has been reported in the weak and intermediate coupling regime when AgNP is located in the line defect region [44] with weakly confined field and larger decays. The total emission rate γ_{tot} of the emitter is divided into three main parts $\gamma_{\mathrm{tot}} = \gamma_{\mathrm{WG}} + \gamma_{\mathrm{abs}} + \gamma_{\mathrm{free}}$ [44] [Fig. 4(a)]: the output part γ_{WG} transmitted to two ends, the absorption part γ_{abs} by the AgNP, and the scattering part γ_{free} leaking to free space. To measure the transmission property, the coupling efficiency is defined as $\beta = \gamma_{\mathrm{WG}}/\gamma_{\mathrm{tot}}$, which describes the useful out-coupling portion in the total emission. β is depicted in the upper inset of Fig. 4(b) as a function of the emitter frequency λ_a when the mode wavelength λ_c is set as 695 nm. The system demonstrates high coupling efficiency, mainly around the cavity resonance. When the emitter is set at $\lambda_a = 696$ nm, $g^{(2)}(0)$ equals 0.025 and the degree of squeezing reaches 0.18 dB. Simultaneously, the major portion of the emission is guided through the line defect with coupling efficiency $\beta = 73.9\%$. Such coupling efficiency reaches the same level in a PhC waveguide [60].

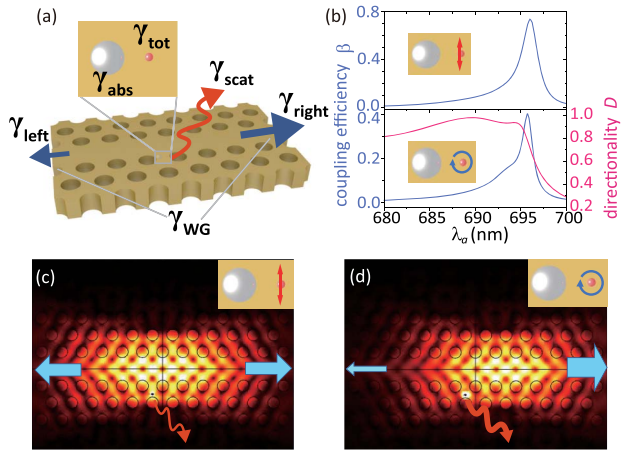

Fig. 4. (a) Schematic diagram of every part of the decay rates. (b) Coupling efficiency β and directionality D excited by a linearly polarized emitter (upper inset) and a circularly polarized emitter (lower inset) in our system. Electric field distributions under excitation of (c) linearly polarized emitter and (d) circularly polarized emitter. The guided part γ_{WG} and scattering part γ_{free} are denoted by blue arrows and red arrows, respectively.

Unidirectional transmission is needed for practical on-chip devices. The spin-locked transmission [61], stemming from the coupling between the transverse spin and a circularly polarized emitter, provides a method to realize such an effect. We use the directionality D [$= \gamma_{\text{right}}/(\gamma_{\text{right}} + \gamma_{\text{left}})$] to measure the unidirectional transmission. As shown in Fig. 4(a), γ_{right}, γ_{left} denote the transmission to the right or left end with $\gamma_{\text{WG}} = \gamma_{\text{right}} + \gamma_{\text{left}}$. The lower inset of Fig. 4(b) indicates that when the coupling efficiency peaks (~40%) in the vicinity of the cavity resonance, the directionality remains at a high level (~90%). As an example, when $\lambda_a = 694.7$ nm and $\lambda_c = 695$ nm, $g^{(2)}(0)$ equals 0.057, the degree of squeezing approaches 0.18 dB, and the directionality D reaches 93% under excitation of a circularly polarized emitter, which indicates the potential of our system to realize on-chip unidirectional transmission of non-classical light. The main source of radiation loss is the leaky part to the lattice region γ_{free} [illustrated in Figs. 4(c) and 4(d)]. It can be further suppressed by changing geometries with truncation of the ends of the line defect [60,62,63]. Unidirectional transmission is also accessible in a weak and an intermediate coupling regimes in a similar system [44]. Intermediate coupling in hybrid plasmonic systems can induce gain without population inversion and double Fano line shapes [64,65].

5. POSSIBILITIES OF EXPERIMENTAL REALIZATIONS

We give some possibilities of experimental realizations of our system below. The material of a PhC waveguide can choose AlGaAs. Its refractive index at 695 nm is close to our settings 51] ($n = 3.3$)]. For strong coupling, the preferable coupling strength g should be greater than 1.2 meV (details in Appendix B), which means the dipole moment reaches $0.3e$ nm or the mode field is more confined. For actual emitters, semiconductor quantum dots [66] may be suitable for our system. The strong coupling between a semiconductor quantum dot and III–V semiconductors has been widely reported [29,66]. For the frequency shift of the band-edge mode via a refractive index, AlGaAs has a large thermo-optic coefficient of 2.3×10^{-4} K^{-1} [51], so the ~1 meV mode shift can be achieved at a very low temperature under 30 K, which is suitable for solid-state quantum dots. The match between lattices of AlGaAs and GaAs quantum dots is also required in experimental preparations. For more confined fields, some hybrid plasmonic structures can be exploited, such as bow-tie resonators [57] and gap plasmon structures [18]. The assembling and positioning of the AgNP and the emitter can be possibly achieved by scanning tunneling microscopy or DNA origami technology [9,49].

6. CONCLUSION

We have theoretically proposed a strongly coupled PhC–plasmonic-emitter system to generate and modulate non-classical light. A strongly confined band-edge mode, which occurs at the band edges of PhCs and possesses a very narrow linewidth, is utilized to realize strong photon–emitter coupling. In such a condition, we have obtained simultaneous single photon and squeezing properties. Modulation of our system can be realized through varying pump frequencies and cavity–emitter detunings, which is feasible in experiments with temperature tuning [50]. The generated non-classical light can be well channeled by a PhC waveguide with high coupling efficiency and unidirectional propagation. The proposal extends the study of non-classical light sources in nanophotonic structures and provides a candidate for a versatile non-classical light source for on-chip applications.

APPENDIX A: DETAILS OF ELECTROMAGNETIC SIMULATION

The numerical simulation is conducted in a PhC waveguide module of 12 rows and 13 columns [Fig. 5(a)] with scattering boundary conditions by COMSOL software using finite element analysis. The geometry scale and the boundary condition ensure that numerical results remain unaffected by the change of module boundaries. The size of the PhC slab is 2210 nm × 1913 nm, which lies between two 500-nm high air layers [Fig. 5(b)], and the height of the PhC layer is 142.8 nm. The wave vectors are mainly restricted in the PhC waveguide on the x–y plane, and the direction of the line defect is defined along x axis. Moreover, a $6a \times 2.5\sqrt{3}a \times 2h$ ($a = 180$ nm, $h = 142.8$ nm) cuboid Σ is set for calculation of the total energy [Fig. 5(c)]. The dipole moment magnitude of the emitter is set at $\mu = 4.4 \times 10^{-13}$ A · m ($1e$ nm). From the numerical results, we obtain the light–atom coupling g, emitter decay γ, and cavity loss κ to describe the strong coupling in the hybrid system. g is calculated as $\vec{\mu} \cdot \vec{E}_{\text{mode}}/\hbar$, where $\vec{E}_{\text{mode}}$ represents the field amplitude corresponding to a single photon excitation. γ is the decay rate to other leaky modes aside from the band-edge mode, which is calculated from the relation $\gamma/\gamma_0 = W/W_0$. γ_0 and W_0 are the decay rate and emitted power in vacuum, respectively. W is the emitted power to other leaky modes, which is acquired by integrating the module surface for Poynting vectors. To get rid of the effect of the output

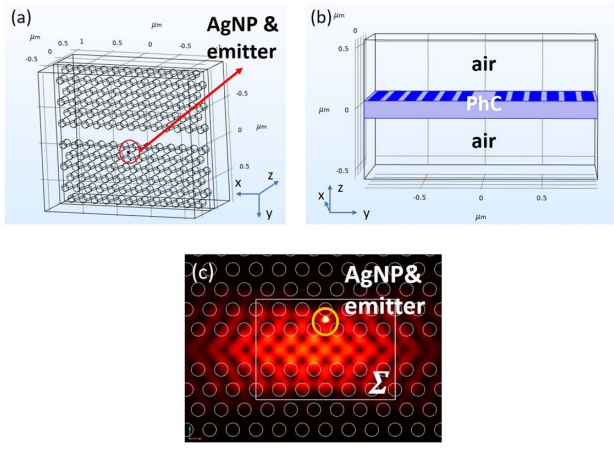

Fig. 5. (a) Schematic diagram of calculation module of strongly coupled photonic-crystal–plasmonic-emitter system. The silver nanoparticle and the emitter are shown by a red circle and an arrow, respectively. (b) Cross section of the module. The PhC layer is between two air layers. (c) Integral region Σ for calculation of total energy Ξ of the band-edge mode. Most of the field excited by the emitter is included in the integral region.

part γ_{WG} from the band-edge mode, the two ends of the waveguide are ruled out in the integral surface. κ is characterized as the full width at half maximum of the absorption spectrum of AgNP.

The integral region Σ contains the AgNP, the emitter, and the PhC waveguide, as shown in Fig. 5(c). The result of electromagnetic energy remains steady when the integral region extends to more PhC cells, which verifies the correctness of such an integral region [44]. The normalized field amplitude $\vec{E}_{\mathrm{mode}}$ is obtained by $\vec{E}_{\mathrm{mode}}(\vec{r}) = \vec{E}(\vec{r})/\sqrt{\Xi/\hbar\omega}$. ω is the band-edge mode frequency, and Ξ represents the energy of the band-edge mode, which is obtained from

$$\Xi = \frac{1}{2}\iiint_{\Sigma}\{\partial_{\omega}[\omega\,\mathrm{Re}\,\varepsilon(\omega)]|_{\omega=\omega_c}|\vec{E}|^2 + \mu_0|\vec{H}|^2\}\mathrm{d}V. \quad \textbf{(A1)}$$

APPENDIX B: PROPERTIES OF THE PHOTON–EMITTER SYSTEM UNDER LOWER DIPOLE MOMENTS

Under experimental conditions, the more common choice of the dipole moment of the emitter is lower than the setting in our system ($1e$ nm). Next, we verify that when $\mu = 0.3 \sim 1e$ nm, the strong coupling regime can be satisfied. Rabi splitting between the band-edge mode and the emitter is depicted in Fig. 6. It can be seen that splitting appears when μ surpasses $0.3e$ nm.

APPENDIX C: ANALYTICAL RESULTS OF THE PHOTON–EMITTER SYSTEM

Below are details of analytical results of coefficients $c_{\alpha,m}$ of the steady-state solution in our system. In the weak excitation condition, $c_{g0} = 1$. The state in our system is limited in two quanta, while the states of more quanta are neglected. That is because the populated probability of every energy eigenstate is $s + m$ orders of pump strength corresponding to the number of quanta, that is, $c_{s,m} \propto \mathcal{E}^{s+m}$. Thus eigenstates with fewer quanta dominate [6]. The evolution of the system is given by Schrödinger equation $i\partial_t\psi = \mathcal{H}\psi$:

$$\begin{aligned}
\dot{c}_{g0} &= 0,\\
\dot{c}_{g1} &= -i\tilde{\Delta}_c c_{g1} - igc_{e0} - i\mathcal{E}c_{e1} \simeq -i\tilde{\Delta}_c c_{g1} - igc_{e0},\\
\dot{c}_{e0} &= -igc_{g1} - i\tilde{\Delta}_a c_{e0} - i\mathcal{E},\\
\dot{c}_{g2} &= -2i\tilde{\Delta}_c c_{g2} - i\sqrt{2}gc_{e1},\\
\dot{c}_{e1} &= -i\sqrt{2}gc_{g2} - i\mathcal{E}c_{g1} - i(\tilde{\Delta}_a + \tilde{\Delta}_c)c_{e1},
\end{aligned} \quad \textbf{(C1)}$$

where $\tilde{\Delta}_a = \Delta_a - i\gamma/2$ and $\tilde{\Delta}_c = \Delta_c - i\kappa/2$. Here the higher-order term $\mathcal{E}c_{e1} \propto \mathcal{E}^3$ is ignored in the expression of $\dot{c}_{g1}$.

The steady-state solutions of the system ($\dot{c}_{\alpha,m} = 0$) are

$$\begin{aligned}
c_{g1} &= \frac{\mathcal{E}g}{\tilde{\Delta}_a\tilde{\Delta}_c - g^2}, \quad c_{e0} = -\frac{\mathcal{E}\tilde{\Delta}_c}{\tilde{\Delta}_a\tilde{\Delta}_c - g^2},\\
c_{g2} &= \frac{\mathcal{E}^2}{\sqrt{2}}\frac{g^2}{(\tilde{\Delta}_a\tilde{\Delta}_c - g^2)[\tilde{\Delta}_c(\tilde{\Delta}_a + \tilde{\Delta}_c) - g^2]},\\
c_{e1} &= -\mathcal{E}^2\frac{g\tilde{\Delta}_c}{(\tilde{\Delta}_a\tilde{\Delta}_c - g^2)[\tilde{\Delta}_c(\tilde{\Delta}_a + \tilde{\Delta}_c) - g^2]}.
\end{aligned} \quad \textbf{(C2)}$$

The eigenenergies of dressed states $\tilde{\Delta}_{n\pm}$ can be calculated from the non-Hermitian Hamiltonian in the two-quanta subspace:

$$\begin{vmatrix}
\tilde{\Delta}_c - \tilde{\Delta}_{n\pm} & g & 0 & 0\\
g & \tilde{\Delta}_a - \tilde{\Delta}_{n\pm} & 0 & 0\\
0 & 0 & 2\tilde{\Delta}_c - \tilde{\Delta}_{n\pm} & \sqrt{2}g\\
\mathcal{E} & 0 & \sqrt{2}g & \tilde{\Delta}_c + \tilde{\Delta}_a - \tilde{\Delta}_{n\pm}
\end{vmatrix} = 0, \quad \textbf{(C3)}$$

and therefore eigenenergies of the effective Hamiltonian can be obtained so that some expressions can be simplified by $\tilde{\Delta}_{1-}\tilde{\Delta}_{1+} = \tilde{\Delta}_a\tilde{\Delta}_c - g^2$ and $\tilde{\Delta}_{2-}\tilde{\Delta}_{2+} = \tilde{\Delta}_c(\tilde{\Delta}_a + \tilde{\Delta}_c) - g^2$. Note that the eigenenergies can also extend to higher energy levels. In the effective Hamiltonian [Eq. (3)] in the main text, the interaction terms between states with the same quanta are in 2×2 submatrices. In other matrix elements, only $\langle e,m|\mathcal{H}_{\mathrm{eff}}|g,m\rangle$ have nonzero values, while $\langle g,m|\mathcal{H}_{\mathrm{eff}}|e,m\rangle$ are ignored because there is the lower probability to de-excite from higher-quanta states to lower-quanta states. So the effective Hamiltonian has the form

$$\begin{bmatrix}
\tilde{\Delta}_c & g & & & & & & \\
g & \tilde{\Delta}_a & & & & & & \\
0 & 0 & 2\tilde{\Delta}_c & \sqrt{2}g & & & & \\
\mathcal{E} & 0 & \sqrt{2}g & \tilde{\Delta}_c + \tilde{\Delta}_a & & & & \\
 & & & & \ddots & & & \\
 & & & & 0 & 0 & \tilde{\Delta}_{g,m} & \sqrt{mg}\\
 & & & & \mathcal{E} & 0 & \sqrt{mg} & \tilde{\Delta}_{e,m-1}\\
 & & & & & & & \ddots
\end{bmatrix}, \quad \textbf{(C4)}$$

where $\tilde{\Delta}_{g,m} = m\tilde{\Delta}_c$, $\tilde{\Delta}_{e,m-1} = \tilde{\Delta}_a + (m-1)\tilde{\Delta}_c$. The eigenenergies can be calculated from its diagonal blocks by some linear algebra calculation:

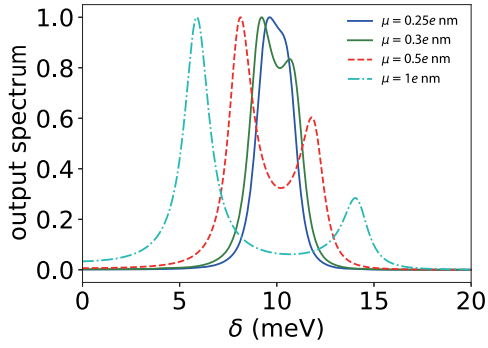

Fig. 6. Output spectrum from the transmitted photon $S(\delta) = \frac{1}{\pi}\mathrm{Re}\int\langle a^{\dagger}(\tau)a(0)\rangle e^{i\delta\tau}\mathrm{d}\tau$ of the band-edge mode when $\mu = 0.25e$ nm, $0.3e$ nm, $0.5e$ nm, $1e$ nm, where Rabi splitting appears when μ is larger than $0.3e$ nm. Here, $\Delta = \Delta_a = \Delta_c$ is set as 10 meV.

$$E_{m\pm} = \frac{\tilde{\Delta}_{g,m} + \tilde{\Delta}_{e,m-1}}{2} \pm \frac{\sqrt{(\tilde{\Delta}_{g,m} - \tilde{\Delta}_{e,m-1})^2 + 4mg^2}}{2}$$
$$= \frac{(2m-1)\tilde{\Delta}_c + \tilde{\Delta}_a}{2} \pm \sqrt{\left(\frac{\tilde{\Delta}_c - \tilde{\Delta}_a}{2}\right)^2 + mg^2}. \quad \text{(C5)}$$

The second-order correlation function $g^{(2)}(0)$ can be expanded by orders of field amplitude $\alpha = \langle a \rangle$ as

$$\begin{aligned}\langle a^{\dagger 2} a^2 \rangle &= \langle (\alpha^* + \Delta a^\dagger)^2 (\alpha + \Delta a)^2 \rangle \\ &= \langle (\alpha^{*2} + 2\alpha^* \Delta a^\dagger + \Delta a^{\dagger 2})(\alpha^2 + 2\alpha \Delta a + \Delta a^2) \rangle \\ &= |\alpha|^4 + 2\,\mathrm{Re}[(\alpha^*)^2 \langle \Delta a^2 \rangle] + 4|\alpha|^2 \langle \Delta a^\dagger \Delta a \rangle \\ &\quad + 4\,\mathrm{Re}[\alpha^* \langle \Delta a^\dagger \Delta a^2 \rangle] + \langle \Delta a^{\dagger 2} \Delta a^2 \rangle \\ &= \langle a^\dagger a \rangle^2 + (\langle \Delta a^{\dagger 2} \Delta a^2 \rangle - \langle \Delta a^\dagger \Delta a \rangle^2) \\ &\quad + 4\,\mathrm{Re}[\alpha^* \langle \Delta a^\dagger \Delta a^2 \rangle] \\ &\quad + 2|\alpha|^2 \langle \Delta a^\dagger \Delta a \rangle + \{2\,\mathrm{Re}[(\alpha^*)^2 \langle \Delta a^2 \rangle]\}, \end{aligned} \quad \text{(C6)}$$

and then $g^{(2)}(0)$ can be split as $1 + I_0 + I_1 + I_2$, with

$$\begin{aligned} I_0 &= \langle \Delta a^{\dagger 2} \Delta a^2 \rangle / \langle a^\dagger a \rangle^2, \\ I_1 &= 4\,\mathrm{Re}[\langle a^\dagger \rangle \langle \Delta a^\dagger \Delta a^2 \rangle] / \langle a^\dagger a \rangle^2, \\ I_2 &= \frac{2|\alpha|^2 \langle \Delta a^\dagger \Delta a \rangle + \alpha^{*2} \langle \Delta a^2 \rangle + \alpha^2 \langle \Delta a^{\dagger 2} \rangle}{\langle a^\dagger a \rangle^2} \\ &= |\alpha|^2 \frac{\langle :(\Delta a^\dagger e^{-i\theta} + \Delta a e^{i\theta})^2 : \rangle}{\langle a^\dagger a \rangle^2} = 4|\alpha|^2 \frac{\langle :\Delta X_\theta^2 : \rangle}{\langle a^\dagger a \rangle^2}. \end{aligned} \quad \text{(C7)}$$

I_0 represents the normally ordered variance of fluctuation intensity, and I_1 represents the normally ordered correlation between fluctuation-field strength and intensity. Particularly, I_2 is proportional to the fluctuation of the quadrature operator, which corresponds to photon squeezing. Therefore, when $I_2 < 0$, the output light has a squeezing property. Substituting Eq. (C2) into Eq. (C7), I_0, I_1, I_2 can be calculated as

$$I_0 = \frac{|\sqrt{2} c_{g2} - c_{g1}^2|^2}{|c_{g1}|^4}, \quad \text{(C8)}$$

$$I_1 = -4 \frac{|c_{g1}|^6}{|c_{g1}|^4}, \quad \text{(C9)}$$

$$I_2 = \frac{2\,\mathrm{Re}[c_{g1}^{*2}(\sqrt{2} c_{g2} - c_{g1}^2)] + 4|c_{g1}|^4 (|c_{g1}|^2 + |c_{e0}|^2)}{|c_{g1}|^4}. \quad \text{(C10)}$$

In the expressions above, terms with orders higher than $\mathcal{E}^6$ are ignored. When the pump is far detuned from resonance, the populations are very small, so the analytical expression with orders of $\mathcal{E}^4$ is enough to describe the non-classical properties. The only exception appears at a photon blockade. The first rungs of dressed states have very large populations due to single photon absorption. So the higher-order terms with only c_{g1}, c_{e0} should be considered. Thus, $g^{(2)}(0)$ and $\langle :\Delta X_\theta^2 : \rangle$ can be deducted from the expressions above, which correspond to Eqs. (4) and (5) in the main text:

$$g^{(2)}(0) = \frac{2|c_{g2}|^2}{|c_{g1}|^4} = \left| \frac{\tilde{\Delta}_{1-} \tilde{\Delta}_{1+}}{\tilde{\Delta}_{2-} \tilde{\Delta}_{2+}} \right|^2, \quad \text{(C11)}$$

$$\begin{aligned} \langle :\Delta X_\theta^2 : \rangle &= \frac{1}{2} \mathrm{Re}\left[e^{-2i\theta} \left(\sqrt{2} c_{g2} - c_{g1}^2 \right) \right] \\ &\quad + |c_{g1}|^2 (|c_{g1}|^2 + |c_{e0}|^2) \\ &= \frac{1}{2} \mathcal{E}^2 g^2 \mathrm{Re}\left[e^{-2i\theta} \frac{\tilde{\Delta}_c^2}{\tilde{\Delta}_{2-} \tilde{\Delta}_{2+} \tilde{\Delta}_{1-}^2 \tilde{\Delta}_{1+}^2} \right] \\ &\quad + \mathcal{E}^4 g^2 \frac{g^2 + |\tilde{\Delta}_c|^2}{|\tilde{\Delta}_{1-} \tilde{\Delta}_{1+}|^4}. \end{aligned} \quad \text{(C12)}$$

APPENDIX D: FURTHER DETAILS OF NON-CLASSICAL LIGHT PROPERTIES

We show further details of non-classical light properties. The state populations are depicted in Fig. 7. At photon antibunching, the system has peak population in the first rungs of dressed states, corresponding to a photon blockade. At photon bunching, the second rungs of dressed states have peak population revealing two-photon absorption, and two-photon absorption occurs even under the photon blockade due to the existence of cavity and emitter decays. This case will weaken single photon properties. In Fig. 8, the second-order correlation function $g^{(2)}(0)$ is calculated with varied emitter decay γ and cavity decay κ. It can be seen that the single photon property is weakened with increasing decays.

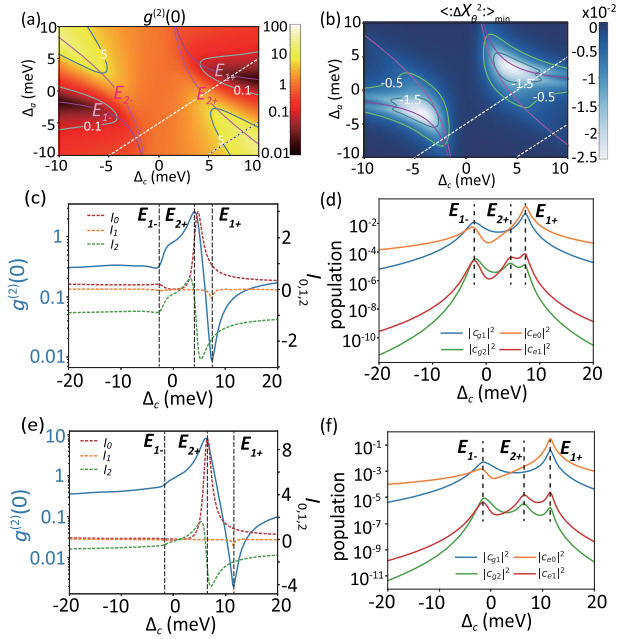

Fig. 7. (a), (b) $g^{(2)}(0)$ and $\langle :\Delta X_\theta^2 : \rangle_{\min}$ with varied Δ_a, Δ_c. Two situations ($\Delta_c - \Delta_a = 5, 10$ meV) are shown by dashed lines, which represent photon bunching with squeezing and without squeezing, respectively. (c), (e) $g^{(2)}(0)$ and $I_{0,1,2}$ when $\Delta_c - \Delta_a = 5, 10$ meV, respectively. (d), (f) State populations when $\Delta_c - \Delta_a = 5, 10$ meV. The vertical dashed lines in (c)–(f) correspond to the first and second rungs of dressed states.

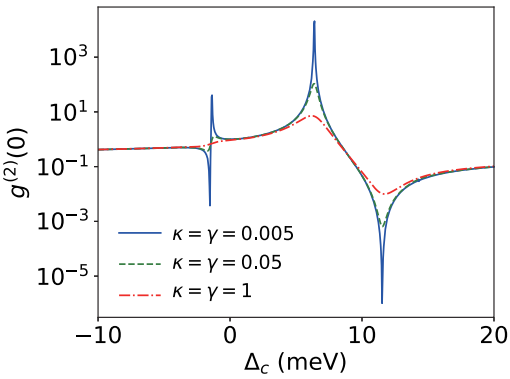

Fig. 8. $g^{(2)}(0)$ as a function of cavity and emitter decays κ, γ. The single photon property is weakened with increasing cavity and emitter decays.

Next, the relation between photon bunching and squeezing is clarified. We choose two typical cases in Fig. 7. In Figs. 7(c) and 7(d), when $\Delta_c - \Delta_a = 5$ meV, the photon bunching and squeezing can be simultaneously obtained. In Figs. 7(e) and 7(f), when $\Delta_c - \Delta_a = 10$ meV, only photon bunching can be achieved. In both cases, photon bunching comes with a negative I_2, which means the existence of photon squeezing ($\langle :\Delta X_\theta^2: \rangle < 0$) at photon bunching. However, $\langle :\Delta X_\theta^2: \rangle \propto I_2 \langle a^\dagger a \rangle^2$ will vanish at larger detunings Δ_c where there are nearly no cavity photons.

It is worth mentioning that only a conventional blockade occurs in our system. It can be verified by the fact that every minimum of $g^{(2)}(0)$ is obtained under single photon excitation, which is the feature of a conventional blockade and rules out the possibility of an unconventional blockade. This is because our system has only an atom driving, where an unconventional blockade is totally suppressed [7].

Funding. National Natural Science Foundation of China (11974032, 11734001, 11525414); Key R&D Program of Guangdong Province (2018B030329001).

Disclosures. The authors declare no conflicts of interest.

Data Availability. Data used to support the findings of this study are included within the paper.

REFERENCES

1. G. Tóth and I. Apellaniz, "Quantum metrology from a quantum information science perspective," J. Phys. A **47**, 424006 (2014).
2. H.-S. Zhong, H. Wang, Y.-H. Deng, M.-C. Chen, L.-C. Peng, Y.-H. Luo, J. Qin, D. Wu, X. Ding, Y. Hu, P. Hu, X.-Y. Yang, W.-J. Zhang, H. Li, Y. Li, X. Jiang, L. Gan, G. Yang, L. You, Z. Wang, L. Li, N.-L. Liu, C.-Y. Lu, and J.-W. Pan, "Quantum computational advantage using photons," Science **370**, 1460–1463 (2020).
3. H. Wang, Y.-M. He, T.-H. Chung, H. Hu, Y. Yu, S. Chen, X. Ding, M.-C. Chen, J. Qin, X. Yang, R.-Z. Liu, Z.-C. Duan, J.-P. Li, S. Gerhardt, K. Winkler, J. Jurkat, L.-J. Wang, N. Gregersen, Y.-H. Huo, Q. Dai, S. Yu, S. Höfling, C.-Y. Lu, and J.-W. Pan, "Towards optimal single-photon sources from polarized microcavities," Nat. Photonics **13**, 770–775 (2019).
4. J. Liu, R. Su, Y. Wei, B. Yao, S. F. Covre da Silva, Y. Yu, J. Iles-Smith, K. Srinivasan, A. Rastelli, J. Li, and X. Wang, "A solid-state source of strongly entangled photon pairs with high brightness and indistinguishability," Nat. Nanotechnol. **14**, 586–593 (2019).
5. M. O. Scully and M. S. Zubairy, *Quantum Optics* (Cambridge University, 1997).
6. H. J. Carmichael, *Statistical Methods in Quantum Optics* (Springer, 2002), Vol. **2**.
7. E. Z. Casalengua, J. C. L. Carreño, F. P. Laussy, and E. del Valle, "Conventional and unconventional photon statistics," Laser Photon. Rev. **14**, 1900279 (2020).
8. E. Z. Casalengua, J. C. L. Carreño, F. P. Laussy, and E. del Valle, "Tuning photon statistics with coherent fields," Phys. Rev. A **101**, 063824 (2020).
9. O. Benson, "Assembly of hybrid photonic architectures from nanophotonic constituents," Nature **480**, 193–199 (2011).
10. A. Imamoğlu, H. Schmidt, G. Woods, and M. Deutsch, "Strongly interacting photons in a nonlinear cavity," Phys. Rev. Lett. **79**, 1467–1470 (1997).
11. A. Faraon, I. Fushman, D. Englund, N. Stoltz, P. Petroff, and J. Vučković, "Coherent generation of non-classical light on a chip via photon-induced tunnelling and blockade," Nat. Phys. **4**, 859–863 (2008).
12. M. G. Raizen, L. A. Orozco, M. Xiao, T. L. Boyd, and H. J. Kimble, "Squeezed-state generation by the normal modes of a coupled system," Phys. Rev. Lett. **59**, 198–201 (1987).
13. T. Yoshie, A. Scherer, J. Hendrickson, G. Khitrova, H. M. Gibbs, G. Rupper, C. Ell, O. B. Shchekin, and D. G. Deppe, "Vacuum Rabi splitting with a single quantum dot in a photonic crystal nanocavity," Nature **432**, 200–203 (2004).
14. J. Topolancik, B. Ilic, and F. Vollmer, "Experimental observation of strong photon localization in disordered photonic crystal waveguides," Phys. Rev. Lett. **99**, 253901 (2007).
15. I. Fushman, D. Englund, A. Faraon, N. Stoltz, P. Petroff, and J. Vučković, "Controlled phase shifts with a single quantum dot," Science **320**, 769–772 (2008).
16. A. Rundquist, M. Bajcsy, A. Majumdar, T. Sarmiento, K. Fischer, K. G. Lagoudakis, S. Buckley, A. Y. Piggott, and J. Vučković, "Nonclassical higher-order photon correlations with a quantum dot strongly coupled to a photonic-crystal nanocavity," Phys. Rev. A **90**, 023846 (2014).
17. K. A. Fischer, K. Müller, A. Rundquist, T. Sarmiento, A. Y. Piggott, Y. Kelaita, C. Dory, K. G. Lagoudakis, and J. Vučković, "Self-homodyne measurement of a dynamic Mollow triplet in the solid state," Nat. Photonics **10**, 163–166 (2016).
18. R. Chikkaraddy, B. De Nijs, F. Benz, S. J. Barrow, O. A. Scherman, E. Rosta, A. Demetriadou, P. Fox, O. Hess, and J. J. Baumberg, "Single-molecule strong coupling at room temperature in plasmonic nanocavities," Nature **535**, 127–130 (2016).
19. J. Ren, Y. Gu, D. Zhao, F. Zhang, T. Zhang, and Q. Gong, "Evanescent-vacuum-enhanced photon-exciton coupling and fluorescence collection," Phys. Rev. Lett. **118**, 073604 (2017).
20. Z. Qian, L. Shan, X. C. Zhang, Q. Liu, Y. Ma, Q. H. Gong, and Y. Gu, "Spontaneous emission in micro- or nanophotonic structures," PhotoniX **2**, 21 (2021).
21. Y.-M. He, Y. He, Y.-J. Wei, D. Wu, M. Atatüre, C. Schneider, S. Höfling, M. Kamp, C.-Y. Lu, and J.-W. Pan, "On-demand semiconductor single-photon source with near-unity indistinguishability," Nat. Nanotechnol. **8**, 213–217 (2013).
21. N. Somaschi, V. Giesz, L. De Santis, J. C. Loredo, M. P. Almeida, G. Hornecker, S. L. Portalupi, T. Grange, C. Antón, J. Demory, C. Gómez, I. Sagnes, N. D. Lanzillotti-Kimura, A. Lemaítre, A. Auffeves, A. G. White, L. Lanco, and P. Senellart, "Near-optimal single-photon sources in the solid state," Nat. Photonics **10**, 340–345 (2016).
23. K. Hennessy, A. Badolato, M. Winger, D. Gerace, M. Atatüre, S. Gulde, S. Fält, E. L. Hu, and A. Imamoğlu, "Quantum nature of a strongly coupled single quantum dot-cavity system," Nature **445**, 896–899 (2007).
24. V. Loo, L. Lanco, A. Lemàtre, I. Sagnes, O. Krebs, P. Voisin, and P. Senellart, "Quantum dot-cavity strong-coupling regime measured through coherent reflection spectroscopy in a very high-Q micropillar," Appl. Phys. Lett. **97**, 241110 (2010).

25. R. Ohta, Y. Ota, M. Nomura, N. Kumagai, S. Ishida, S. Iwamoto, and Y. Arakawa, "Strong coupling between a photonic crystal nanobeam cavity and a single quantum dot," Appl. Phys. Lett. **98**, 173104 (2011).
26. J. P. Reithmaier, G. Sęk, A. Löffler, C. Hofmann, S. Kuhn, S. Reitzenstein, L. V. Keldysh, V. D. Kulakovskii, T. L. Reinecke, and A. Forchel, "Strong coupling in a single quantum dot–semiconductor microcavity system," Nature **432**, 197–200 (2004).
27. J. Kasprzak, S. Reitzenstein, E. A. Muljarov, C. Kistner, C. Schneider, M. Strauss, S. Höfling, A. Forchel, and W. Langbein, "Up on the Jaynes–Cummings ladder of a quantum-dot/microcavity system," Nat. Mater. **9**, 304–308 (2010).
28. H. Wang, J. Qin, S. Chen, M.-C. Chen, X. You, X. Ding, Y.-H. Huo, Y. Yu, C. Schneider, S. Höfling, M. Scully, C.-Y. Lu, and J.-W. Pan, "Observation of intensity squeezing in resonance fluorescence from a solid-state device," Phys. Rev. Lett. **125**, 153601 (2020).
29. E. Peter, P. Senellart, D. Martrou, A. Lemaître, J. Hours, J. M. Gérard, and J. Bloch, "Exciton-photon strong-coupling regime for a single quantum dot embedded in a microcavity," Phys. Rev. Lett. **95**, 067401 (2005).
30. K. Srinivasan and O. Painter, "Linear and nonlinear optical spectroscopy of a strongly coupled microdisk-quantum dot system," Nature **450**, 862–865 (2007).
31. B. Min, E. Ostby, V. Sorger, E. Ulin-Avila, L. Yang, X. Zhang, and K. Vahala, "High-*Q* surface-plasmon-polariton whispering-gallery microcavity," Nature **457**, 455–458 (2009).
32. A. Huck, S. Smolka, P. Lodahl, A. S. Sørensen, A. Boltasseva, J. Janousek, and U. L. Andersen, "Demonstration of quadrature-squeezed surface plasmons in a gold waveguide," Phys. Rev. Lett. **102**, 246802 (2009).
33. K. Santhosh, O. Bitton, L. Chuntonov, and G. Haran, "Vacuum Rabi splitting in a plasmonic cavity at the single quantum emitter limit," Nat. Commun. **7**, 11823 (2016).
34. R. Liu, Z.-K. Zhou, Y.-C. Yu, T. Zhang, H. Wang, G. Liu, Y. Wei, H. Chen, and X.-H. Wang, "Strong light-matter interactions in single open plasmonic nanocavities at the quantum optics limit," Phys. Rev. Lett. **118**, 237401 (2017).
35. R. Bose, D. Sridharan, H. Kim, G. S. Solomon, and E. Waks, "Low-photon-number optical switching with a single quantum dot coupled to a photonic crystal cavity," Phys. Rev. Lett. **108**, 227402 (2012).
36. A. Reinhard, T. Volz, M. Winger, A. Badolato, K. J. Hennessy, E. L. Hu, and A. Imamoğlu, "Strongly correlated photons on a chip," Nat. Photonics **6**, 93–96 (2012).
37. T. Volz, A. Reinhard, M. Winger, A. Badolato, K. J. Hennessy, E. L. Hu, and A. Imamoğlu, "Ultrafast all-optical switching by single photons," Nat. Photonics **6**, 605–609 (2012).
38. D. Englund, A. Majumdar, M. Bajcsy, A. Faraon, P. Petroff, and J. Vučković, "Ultrafast photon-photon interaction in a strongly coupled quantum dot-cavity system," Phys. Rev. Lett. **108**, 093604 (2012).
39. K. Müller, A. Rundquist, K. A. Fischer, T. Sarmiento, K. G. Lagoudakis, Y. A. Kelaita, C. Sánchez Muñoz, E. Del Valle, F. P. Laussy, and J. Vučković, "Coherent generation of nonclassical light on chip via detuned photon blockade," Phys. Rev. Lett. **114**, 233601 (2015).
40. H. Flayac, D. Gerace, and V. Savona, "An all-silicon single-photon source by unconventional photon blockade," Sci. Rep. **5**, 11223 (2015).
41. X.-L. Chu, S. Götzinger, and V. Sandoghdar, "A single molecule as a high-fidelity photon gun for producing intensity-squeezed light," Nat. Photonics **11**, 58–62 (2017).
42. C. H. H. Schulte, J. Hansom, A. E. Jones, C. Matthiesen, C. Le Gall, and M. Atatüre, "Quadrature squeezed photons from a two-level system," Nature **525**, 222–225 (2015).
43. H.-P. Gauggel, H. Artmann, C. Geng, F. Scholz, and H. Schweizer, "Wide-range tunability of GaInP-AlGaInP DFB lasers with superstructure gratings," IEEE Photon. Technol. Lett. **9**, 14–16 (1997).
44. F. Zhang, J. Ren, L. Shan, X. Duan, Y. Li, T. Zhang, Q. Gong, and Y. Gu, "Chiral cavity quantum electrodynamics with coupled nanophotonic structures," Phys. Rev. A **100**, 053841 (2019).
45. P. Peng, Y.-C. Liu, D. Xu, Q.-T. Cao, G. Lu, Q. Gong, and Y.-F. Xiao, "Enhancing coherent light-matter interactions through microcavity-engineered plasmonic resonances," Phys. Rev. Lett. **119**, 233901 (2017).
46. H.-J. Chen, "Auxiliary-cavity-assisted vacuum Rabi splitting of a semiconductor quantum dot in a photonic crystal nanocavity," Photon. Res. **6**, 1171–1176 (2018).
47. Y.-W. Lu, J.-F. Liu, Z. Liao, and X.-H. Wang, "Plasmonic-photonic cavity for high-efficiency single-photon blockade," Sci. China Phys. Mech. Astron. **64**, 274212 (2021).
48. P. B. Johnson and R. W. Christy, "Optical constants of the noble metals," Phys. Rev. B **6**, 4370–4379 (1972).
49. X. Shen, C. Song, J. Wang, D. Shi, Z. Wang, N. Liu, and B. Ding, "Rolling up gold nanoparticle-dressed DNA origami into three-dimensional plasmonic chiral nanostructures," J. Am. Chem. Soc. **134**, 146–149 (2011).
50. D. Englund, A. Faraon, I. Fushman, N. Stoltz, P. Petroff, and J. Vučković, "Controlling cavity reflectivity with a single quantum dot," Nature **450**, 857–861 (2007).
51. L. Chang, W. Xie, H. Shu, Q.-F. Yang, B. Shen, A. Boes, J. D. Peters, W. Jin, C. Xiang, S. Liu, G. Moille, S.-P. Yu, X. Wang, K. Srinivasan, S. B. Papp, K. Vahala, and J. E. Bowers, "Ultra-efficient frequency comb generation in AlGaAs-on-insulator microresonators," Nat. Commun. **11**, 1331 (2020).
52. F. P. Laussy, E. del Valle, M. Schrapp, A. Laucht, and J. J. Finley, "Climbing the Jaynes–Cummings ladder by photon counting," J. Nanophoton. **6**, 061803 (2012).
53. J. Johansson, P. Nation, and F. Nori, "QuTiP: an open-source python framework for the dynamics of open quantum systems," Comput. Phys. Commun. **183**, 1760–1772 (2012).
54. J. Johansson, P. Nation, and F. Nori, "QuTiP 2: a Python framework for the dynamics of open quantum systems," Comput. Phys. Commun. **184**, 1234–1240 (2013).
55. R. Trivedi, K. A. Fischer, J. Vučković, and K. Müller, "Generation of non-classical light using semiconductor quantum dots," Adv. Quantum. Technol. **3**, 1900007 (2020).
56. M. Arcari, I. Söllner, A. Javadi, S. L. Hansen, S. Mahmoodian, J. Liu, H. Thyrrestrup, E. H. Lee, J. D. Song, S. Stobbe, and P. Lodahl, "Near-unity coupling efficiency of a quantum emitter to a photonic crystal waveguide," Phys. Rev. Lett. **113**, 093603 (2014).
57. A. Kinkhabwala, Z. Yu, S. Fan, Y. Avlasevich, K. Müllen, and W. E. Moerner, "Large single-molecule fluorescence enhancements produced by a bowtie nanoantenna," Nat. Photonics **3**, 654–657 (2009).
58. F. Zhang, J. Ren, X. Duan, Z. Chen, Q. Gong, and Y. Gu, "Evanescent-field-modulated two-qubit entanglement in an emitters-plasmon coupled system," J. Phys. Condens. Matter **30**, 305302 (2018).
59. F. Zhang, D. Zhao, X. Hu, Q. Gong, and Y. Gu, "Quantum discord modulated by detuning in a plasmonic nanosystem," J. Phys. B **52**, 115402 (2019).
60. V. S. C. Manga Rao and S. Hughes, "Numerical study of exact Purcell factors in finite-size planar photonic crystal waveguides," Opt. Lett. **33**, 1587–1589 (2008).
61. T. Van Mechelen and Z. Jacob, "Universal spin-momentum locking of evanescent waves," Optica **3**, 118–126 (2016).
62. H. Thyrrestrup, L. Sapienza, and P. Lodahl, "Extraction of the β-factor for single quantum dots coupled to a photonic crystal waveguide," Appl. Phys. Lett. **96**, 231106 (2010).
63. C. Li, X. Zhang, J. W. Li, T. Fang, and X. W. Dong, "The challenges of modern computing and new opportunities for optics," PhotoniX **2**, 20 (2021).
64. D. Zhao, Y. Gu, J. Wu, J. Zhang, T. Zhang, B. D. Gerardot, and Q. Gong, "Quantum-dot gain without inversion: effects of dark plasmon-exciton hybridization," Phys. Rev. B **89**, 245433 (2014).
65. D. Zhao, J. Wu, Y. Gu, and Q. Gong, "Tailoring double Fano profiles with plasmon-assisted quantum interference in hybrid exciton-plasmon system," Appl. Phys. Lett. **105**, 111112 (2014).
66. P. Lodahl, S. Mahmoodian, and S. Stobbe, "Interfacing single photons and single quantum dots with photonic nanostructures," Rev. Mod. Phys. **87**, 347–400 (2015).